PCCP

Extracting accurate information from triplet-triplet annihilation upconversion data with a mass-conserving kinetic model

Journal:	*Physical Chemistry Chemical Physics*
Manuscript ID	CP-ART-08-2022-003986.R1
Article Type:	Paper
Date Submitted by the Author:	10-Nov-2022
Complete List of Authors:	Fourkas, John; University of Maryland Kalpattu, Abhishek; University of Maryland Hanson, Kenneth; Florida State University Dilbeck, Tristan; Florida State University

Extracting accurate information from triplet-triplet annihilation upconversion data with a mass-conserving kinetic model

Abhishek Kalpattu,[a] Tristan Dilbeck,[b] Kenneth Hanson,[b] and John T. Fourkas*[c,d,e]

[a]Department of Materials Science and Engineering, University of Maryland, College Park, MD 20817, USA

[b]Department of Chemistry and Biochemistry, Florida State University, Tallahassee, FL 32306 USA

[c]Department of Chemistry and Biochemistry, University of Maryland, College Park, MD 20817, USA

[d]Institute for Physical Science and Technology, University of Maryland, College Park, MD 20817, USA

[e]Maryland Quantum Materials Center, University of Maryland, College Park, MD 20817, USA

*To whom correspondence should be addressed, fourkas@umd.edu

Abstract

Triplet-triplet annihilation upconversion (TTA-UC) is a process that shows promise for applications such as energy-harvesting and light-generation technologies. The irradiance dependent performance of TTA-UC systems is typically gauged using a graphical analysis, rather than a detailed model. Additionally, kinetic models for TTA-UC rarely incorporate mass conservation, which is a phenomenon that can have important consequences under experimentally relevant conditions. We present an analytical, mass-conserving kinetic model for TTA-UC, and demonstrate that the mass-conservation constraint cannot generally be ignored. This model accounts for saturation in TTA-UC data. Saturation complicates the interpretation of the threshold irradiance I_{th}, a popular performance metric. We propose two alternative figures of merit for overall performance. Finally, we show that our model can robustly fit experimental data from a wide variety of sensitized TTA-UC systems, enabling the direct and accurate determination of I_{th} and of our proposed performance metrics. We employ this fitting procedure to benchmark and compare these metrics, using data from the literature.

Table of rate constants and variables

Variable	Explanation	Variable	Explanation
$[S]$	Concentration of ground-state sensitizers	$[A]$	Concentration of ground-state annihilators
$[^1S^*]$	Concentration of sensitizers in first excited singlet state	$[^1A^*]$	Concentration of annihilators in the first excited singlet state
$[^3S^*]$	Concentration of sensitizers in the lowest triplet state	$[^3A^*]$	Concentration of annihilators in the lowest triplet state
$[^3A^{**}]$	Concentration of annihilators in a higher-order triplet state	β	Fraction of annihilator triplets decaying initially through TTA
B_{ISC}	Irradiance dependent yield of sensitizer intersystem crossing	β_{ISC}	Branching ratio for sensitizer intersystem crossing
B_{sens}	Irradiance dependent yield of triplet sensitization	β_{sens}	Branching ratio of sensitization from the sensitizer
β_{RISC}	Branching ratio for annihilator reverse intersystem crossing	δ_I	Percent difference between fit and graphically determined values of I_{th}
δ_n	Percent difference between fit and ideal values of $n(I_{th})$	F_{SS}	Steady-state fluorescence rate
$F_{SS,\,low}$	Steady-state fluorescence rate in the low-irradiance regime	$F_{SS,\,high}$	Steady-state fluorescence rate in the high-irradiance regime
$F_{SS,\,sat}$	Steady-state fluorescence rate in the saturation regime	$\overline{F}_{SS}$	Normalized steady-state fluorescence rate
Φ_{fl}	Fluorescence quantum yield	Φ_{UC}	TTA-UC quantum yield (photons out divided by photons in)
$\Phi_{UC,max}$	The maximum attainable value of Φ_{UC} for any given TTA-UC system	$\overline{\Phi}_{UC}$	$\Phi_{UC}/\Phi_{UC,max}$
Γ	The range of irradiances at which a TTA-UC system performs optimally	I	Irradiance
I_{cr}	The point at which an extrapolated line with a slope of 2 on a logarithmic curve intersects $F_{SS,\,sat}$	I_n	The irradiance at which the local slope is n
I_{sat}	The cross-over point between the high irradiance and saturation regions	I_{th}	The threshold irradiance
k_{ex}	Rate constant for photoexcitation of the sensitizer	k_{fl}	Rate constant for annihilator fluorescence
k_{IC}	Rate constant for internal conversion in the annihilator	k_{ISC} (k_{ISC}')	Intersystem crossing rate constant for the sensitizer (annihilator)
k_{NR}^A	Rate constant for singlet non-radiative decay in the annihilator	k_{NR}^S	Rate constant for singlet non-radiative decay in the sensitizer
k_{RISC}	Rate constant for reverse intersystem crossing in the annihilator	k_{sens}	Rate constant for sensitization of the annihilator by the sensitizer
k_T^A	Pseudo-first-order rate constant for annihilator triplet quenching	k_T^S	Pseudo-first-order rate constant for sensitizer triplet quenching
k_{TTA}	Triplet-triplet annihilation rate constant	$n(I)$	The slope for a given I in a plot of log (I) vs. log (F_{SS})
ξ	I_{th}/I_{cr}	R_{sens}	Overall rate of triplet sensitization
ρ	Second term in the radicand in the expression for F_{SS} in eqn 14	ψ	$\log(I_{th})/(\log(I_{sat}) - \log(I_{th}))$

Introduction

Triplet-triplet annihilation upconversion (TTA-UC) is a term used to describe a singlet excited state that is formed via the disproportionation of two triplet excited states.[1, 2] In a typical TTA-UC process, a photoexcited sensitizer (*S*) singlet state undergoes intersystem crossing (ISC) to the lowest triplet excited state. Triplet energy transfer then takes place between the sensitizer and an annihilator (*A*).[2, 3] The collision of two annihilators in their lowest triplet states can result in the formation of a singlet excited state that fluoresces at a wavelength that is shorter than that of the light used to excite the sensitizers. Although TTA-UC was first described in 1962 in phenanthrene/anthracene systems,[4] there has been a recent surge in interest in this field, owing to the discovery of organometallic compounds in which long-lived triplet states can be photogenerated efficiently at room temperature.[5-8] The intensity of the upconverted fluorescence is affected strongly by phenomena such as annihilator triplet quenching (for which we denote the rate constant k_T^A) and triplet-triplet annihilation (for which we denote the rate constant k_{TTA}). The overall efficiency of the TTA-UC process is determined primarily by the sensitization rate (for which we denote the rate constant k_{sens}) and the pseudo-first-order sensitizer triplet quenching rate (for which we denote the rate constant k_T^S).

Over the past decade, a number of different kinetic frameworks have been developed to describe TTA-UC. Monguzzi *et al*. analyzed a series of coupled rate equations at steady state to show that when the product of k_T^A and the annihilator triplet concentration, $[^3A^*]$, is much larger than the product $k_{TTA}[^3A^*]^2$, a quadratic relationship exists between the upconverted fluorescence intensity and the irradiance (which the authors defined as I_{UC} and I_{exc}, respectively).[9] Conversely, they showed that when $k_T^A[^3A^*] \ll k_{TTA}[^3A^*]^2$, I_{UC} depends linearly on I_{exc}. The point at which the quadratic and linear regions meet is known as the threshold irradiance (I_{th}), which is often interpreted to be point at which, on average, 50% of the

annihilator molecules undergo TTA.[10, 11] Monguzzi *et al*.[9] derived an expression for I_{th} by equating their results for I_{UC} in the low and high I_{exc} limits.

Haefele *et al*. presented a time-dependent solution of kinetic rate equations to describe the change in annihilator triplet concentration in terms of simultaneous loss through intrinsic triplet quenching and TTA.[12] These authors evaluated their analytical solution under a set of kinetic limits that were nearly identical to those of Monguzzi *et al*. Schmidt and co-workers have also developed a number of models to describe the behavior of TTA-UC.[3, 13, 14] One of these models suggests that the efficiency of the TTA-UC process depends on a competition between the intrinsic decay of sensitizer triplets and the product $k_{sens}[A]_t$, where $[A]_t$ is the concentration of ground-state annihilators at time *t*. This result is notable, as most researchers have only considered k_{sens} as part of a branching ratio $\beta_{sens} = \frac{k_{sens}}{k_{sens} + k_T^S}$. Uniquely, Schmidt and co-workers also considered heterogenous TTA processes between triplets from the sensitizer and annihilator.[13]

Murakami and Kamada have recently presented a kinetic treatment of the TTA-UC process in which they discuss the effects of ISC from the annihilator excited singlet state $[^1A^*]$ to the annihilator triplet state $[^3A^*]$, as well as the effects of spin statistics.[15] These authors also dispelled the notion that I_{th} represents the point at which the TTA process reaches half of its maximum efficiency.

Although considerable advances have been made in understanding the nature of TTA-UC systems from a kinetic standpoint, most analytical treatments have focused on limiting behaviors. Moreover, the kinetic limits in which a TTA-UC system exhibits quadratic and linear dependences on irradiance are often given in terms of $[^3A^*]$, which is a complex quantity that is not easily accessible experimentally, and that depends on the irradiance and system parameters. Equations that instead incorporate the initial concentrations of the species when

the system is not being irradiated are more readily evaluated. Finally, existing treatments have not incorporated mass conservation, and so cannot model saturation behavior.

Here we present a detailed kinetic model of the TTA-UC process that includes mass conservation, and we use this model to find analytical expressions for the steady-state concentrations of key species. We demonstrate that mass conservation significantly alters some the conclusions of a thorough kinetic analysis. Our approach allows us to express kinetic limits in terms of readily obtainable rate constants and the known initial annihilator and sensitizer concentrations, $[A]_0$ and $[S]_0$, respectively. Furthermore, this model can be used to examine non-ideal implementations of TTA-UC. In particular, we show that a linear dependence between the steady-state fluorescence rate F_{ss} and the irradiance I exists only for a limited range of irradiance. We further demonstrate that F_{ss} is limited by the finite values of k_{sens} and $[A]_0$, resulting in the saturation of upconverted fluorescence at high irradiance. Moreover, although I_{th} has often been considered as a key parameter in characterizing the efficiency of the TTA-UC process, we demonstrate that it is difficult to determine I_{th} reliably through the conventional analysis of TTA-UC data. Additionally, in the presence of saturation, I_{th} is not necessarily an ideal performance metric. We therefore propose two new performance metrics and demonstrate the feasibility of determining all three of these metrics accurately by applying our kinetic expression for the dependence of F_{ss} on irradiance to fit experimental data. We demonstrate the utility of this approach on experimental data reported for wide a range of TTA-UC data from the literature.

Experimental

TTA-UC experiments

9,10-diphenylanthracene (DPA, Sigma-Aldrich), platinum octaethylporphyrin (PtOEP, Frontier Scientific), and toluene (Alfa Aesar) were used as received. Samples were prepared

by dissolving the platinum porphyrin sensitizer and anthracene annihilator molecules in toluene in a 1 cm × 1 cm quartz cuvette. The samples were then sealed with rubber septa, bubble deaereated with N_2 gas for 30 min, and measured immediately to minimize the introduction of oxygen into the system during data acquisition.

Data were collected at room temperature using an Edinburgh FLS980 fluorescence spectrometer. The samples were excited using the 532 nm output from a Nd:YAG laser (Aixiz, AD-532-400T). The laser output was passed through a variable neutral density filter (Edinburgh F-B01 laser mount) and a 2-mm-diameter iris (Newport ID-1.0), and then directed to the sample via a flip mirror. Emission from the sample was first passed through a 532 nm notch filter (Thorlabs Inc., NF533-17) then a single grating (1800 lines/mm, 500 nm blaze) Czerny-Turner monochromator, and was detected by a Peltier-cooled Hamamatsu R928 photomultiplier tube. Laser powers were measured using a power meter (Ophir Vega 7Z01560) with a high sensitivity sensor (Ophir 3A-FS 7Z02628).

Data fitting

Data fitting was performed with MATLAB's Curve Fitting Toolbox. Known parameter values were substituted into the expression derived below for F_{SS} to generate a fitting equation. The resultant fitting equation was simplified by assuming the fractional yield of sensitizer triplets through ISC to be unity, and ISC and reverse intersystem crossing (RISC) events in the annihilator to be negligible. Because upconverted fluorescence intensity values are arbitrary, and often vary depending on the instrumentation used, the upconverted fluorescence intensity was normalized to the highest experimental value prior to fitting. A weighting factor of $1/\overline{F}_{SS}(I)$ was applied to the fits, where $\overline{F}_{SS}(I)$ is the normalized upconverted fluorescence intensity at irradiance *I*, to ensure that the data points at all irradiances are treated equally when fitting.

Results and discussion

The kinetic model

Schematics of the processes considered in our kinetic model are shown in Fig. 1. The rate equations for the time evolution of $[^1S^*]$, $[^3S^*]$, $[^1A^*]$, $[^3A^{**}]$ and $[^3A^*]$ in terms of the concentrations of the sensitizer ground state $[S]$ and the annihilator ground state $[A]$ are

$$\frac{d[^1S^*]}{dt} = k_{ex}I[S] - k_{NR}^S[^1S^*] - k_{ISC}[^1S^*] \quad (1)$$

$$\frac{d[^3S]}{dt} = k_{ISC}[^1S^*] - k_{sens}[^3S^*][A] - k_T^S[^3S^*] \quad (2)$$

$$\frac{d[^3A^*]}{dt} = k_{sens}[^3S^*][A] + k_{ISC}'[^1A^*] - k_T^A[^3A^*] - 2k_{TTA}[^3A^*]^2 + k_{IC}[^3A^{**}] \quad (3)$$

$$\frac{d[^3A^{**}]}{dt} = 0.75k_{TTA}[^3A^*]^2 - k_{RISC}[^3A^{**}] - k_{IC}[^3A^{**}]\,. \quad (4)$$

and

$$\frac{d[^1A^*]}{dt} = 0.25k_{TTA}[^3A^*]^2 + k_{RISC}[^3A^{**}] - \left(k_{fl} + k_{NR}^A + k_{ISC}'\right)[^1A^*]\,. \quad (5)$$

Here, the term $k_{ex}I$ is the rate constant for the excitation process times the irradiance (I), k_{NR}^S is the rate constant for all first-order or pseudo-first-order decay mechanisms for $^1S^*$ except for intersystem crossing (ISC), and k_{ISC} is the rate constant for ISC to T_1. The term $k_{sens}[^3S^*][A]$ represents the rate of triplet sensitization of an annihilator. The rate constants k_T^S and k_T^A are for all first-order or pseudo-first-order triplet decay mechanisms in the sensitizer and annihilator, respectively. The rate constant k_{ISC}' governs the repopulation of $^3A^*$ through ISC from $^1A^*$, k_{TTA} is the rate constant for TTA, and k_{IC} is the rate constant for internal conversion from $^3A^{**}$ to $^3A^*$. The coefficients that precede the k_{TTA} terms arise from spin statistics, as discussed in the next section. The rate constant for fluorescence from $^1A^*$ is k_{fl}. The rate constant k_{RISC} governs RISC from $^3A^{**}$ to $^1A^*$.

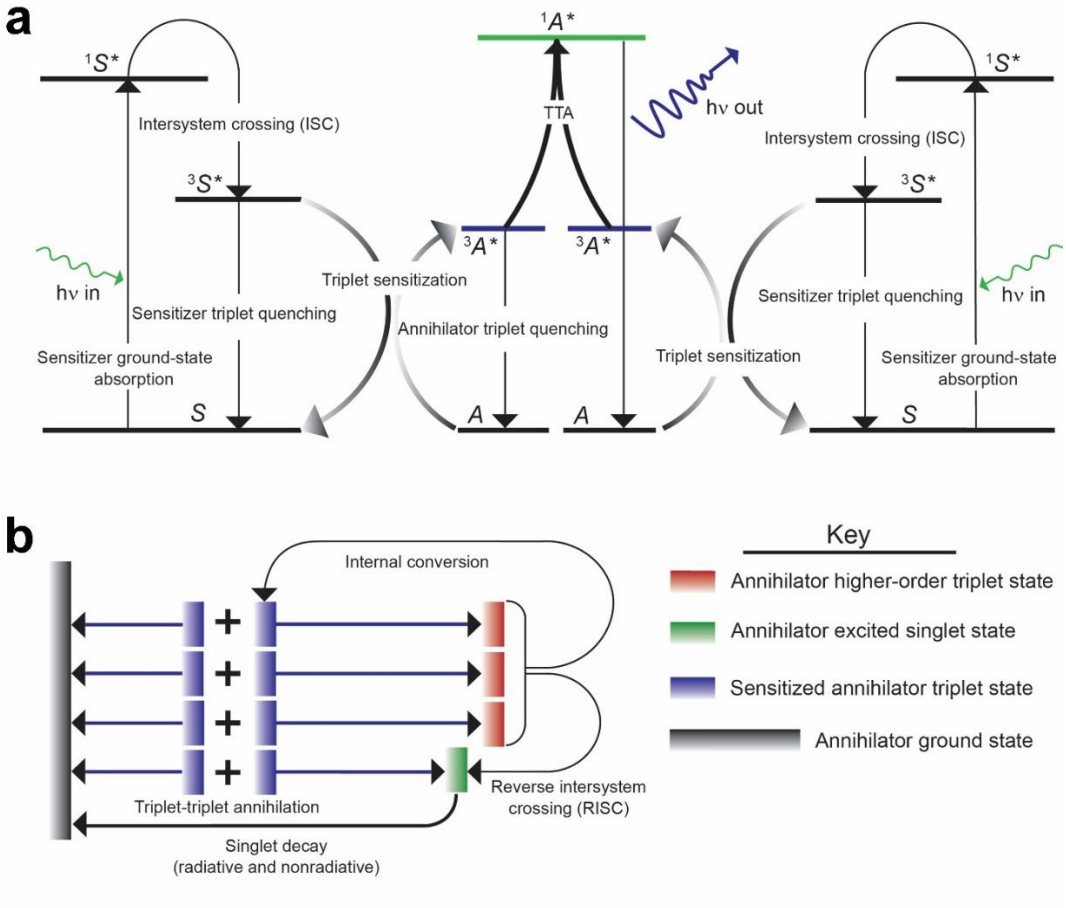

Fig. 1 Schematics of the processes considered in the TTA-UC kinetic model. (a) Photoexcited sensitizers undergo intersystem crossing from the lowest singlet excited state (denoted $^1S^*$) to the lowest sensitizer triplet state ($^3S^*$). Triplet sensitization by $^3S^*$ generates an annihilator triplet state ($^3A^*$). Two annihilators in their triplet states can undergo TTA to generate one annihilator in its ground state (A) and another in a singlet excited state ($^1A^*$), the latter of which can emit at a wavelength shorter than that of the excitation light. (b) Spin-statistics-based outcomes of triplet-triplet annihilation when no quintet state is energetically accessible. This annihilation event will create a ground state and an excited singlet state 25% of the time, and a ground state and a higher-order excited triplet state 75% of the time. In the latter case, the high energy triplet typically undergoes internal conversion to $^3A^*$. However, reverse intersystem crossing can also take the higher-order triplet state to the singlet manifold, from which the molecule can fluoresce.

We also employ two mass-conservation equations,

$$[S]_t = [S]_0 - [^3S^*]_t - [^1S^*]_t \tag{6}$$

and

$$[A]_t = [A]_0 - [^3A^*]_t - [^1A^*]_t - [^3A^{**}]_t \ . \tag{7}$$

These equations are crucial for developing analytical expressions for all of the steady-state concentrations of species in terms of the known initial concentrations of $[S]_0$ and $[A]_0$.

We solve all of the rate equations at steady state by setting the rate of change of the population of each species to zero. Expressions for the steady-state concentrations of $[^1S^*]$ and $[^3S^*]$ are given in the ESI. The rate of upconverted fluorescence is

$$F_{SS} = k_{fl}[^1A^*]_{SS} = \frac{k_{fl}k_{TTA}[^3A^*]_{SS}^2\left(1+\frac{k_{RISC}}{k_{IC}+k_{RISC}}\right)}{4(k_{fl}+k_{NR}^A+k_{ISC}')} \ . \tag{8}$$

F_{SS} is proportional to the experimentally measured upconverted fluorescence intensity. The steady-state solution for the concentration of annihilator triplets can be written as

$$\frac{B_{ISC}k_{sens}k_{ex}I[S]_0}{B_{ISC}k_{ex}I + k_{sens}[A]_{SS} + k_T^S}\left([A]_0 - [^3A^*]_{SS} - \frac{k_{TTA}[^3A^*]_{SS}^2\left(1+\frac{k_{RISC}}{k_{IC}+k_{RISC}}\right)}{4(k_{fl}+k_{NR}^A+k_{ISC}')} - \frac{0.75k_{TTA}[^3A^*]_{SS}^2}{k_{IC}+k_{RISC}}\right)$$

$$= k_T^A[^3A^*]_{SS} + \left(1.25+\frac{k_{RISC}}{k_{IC}+k_{RISC}}\right)k_{TTA}[^3A^*]_{SS}^2 - k_{ISC}'\frac{k_{TTA}[^3A^*]_{SS}^2\left(1+\frac{k_{RISC}}{k_{RISC}+k_{IC}}\right)}{4(k_{fl}+k_{NR}^A+k_{ISC}')} \ . \tag{9}$$

Here, B_{ISC} is an irradiance dependent ratio that is defined as

$$B_{ISC} = \frac{k_{ISC}}{k_{ISC}+k_{ex}I+k_{NR}^S} \ . \tag{10}$$

Although TTA between sensitizer triplets could be included in this model, we ignore this effect in our analysis, because under typical conditions the concentration of ground-state annihilators is considerably higher than the concentration of excited sensitizers. A more detailed analysis of the conditions under which sensitizer TTA could be important is provided in the ESI (see Fig. S1). We can solve eqn (9) through either an approximate approach or an exact approach. The former strategy involves the assumption that $[A]_{SS} \cong [A]_0$, which follows from the typical situation in TTA-UC in solution that $[A]_0 \gg [S]_0$. This approach results in a quadratic equation for $[^3A^*]_{SS}$, and so we denote the resultant expression the quadratic model. In the second strategy, eqn (7) can be used to determine $[^3S^*]_{SS}$. In this case, eqn (9) takes on a quartic form that can be solved analytically for $[^3A^*]_{SS}$, yielding one positive root of interest, as well as three negative roots. We denote the resultant, complex expression the quartic model.

In the quartic model, the rate at which triplets are supplied to the annihilator is $k_{sens}[^3S^*][A]$, which, under steady-state conditions, is given by

$$k_{sens}[^3S^*]_{SS}[A]_{SS} =$$

$$k_{sens}[^3S^*]_{SS}\left([A]_0 - [^3A^*]_{SS} - \frac{0.75k_{TTA}[^3A^*]_{SS}^2}{k_{IC}+k_{RISC}} - \frac{k_{TTA}[^3A^*]_{SS}^2\left(1+\frac{k_{RISC}}{k_{IC}+k_{RISC}}\right)}{4\left(k_{fl}+k_{NR}^A+k_{ISC}'\right)}\right) \quad (11)$$

In the quadratic model, $k_{sens}[^3S^*]_{SS}[A]_{SS}$ reduces to $k_{sens}[^3S^*]_{SS}[A]_0$. Because $[^3A^*]_{SS}$ increases with *I*, the rate of sensitization becomes smaller at higher irradiance in the quartic model. This situation opens up a saturation pathway for upconverted fluorescence that Monguzzi *et al*. discussed previously, but did not model with rate equations.[10]

In Fig. 2 we compare the results of the quadratic and quartic models for solutions with $[A]_0$ = 100 mM and $[S]_0$ = 14 mM or 0.14 mM (see Table S1 for a list of parameter values in all

figures in this paper). When k_T^A, k_{sens}, and k_{TTA} are fixed at 2.00 × 10^2 s^{-1}, 1.63 × 10^9 M^{-1} s^{-1}, and 3.6 × 10^8 M^{-1} s^{-1}, respectively, the two models are nearly indistinguishable (Fig. 2a). When k_{TTA} is reduced by four orders of magnitude, the resultant accumulation of annihilator triplets leads to notable fluorescence saturation at high irradiance, as seen in Fig. 2b. The quartic model exhibits a more rapid transition to fluorescence saturation than does the quadratic model, particularly when the expenditure of annihilator triplets through intrinsic decay or TTA is small.

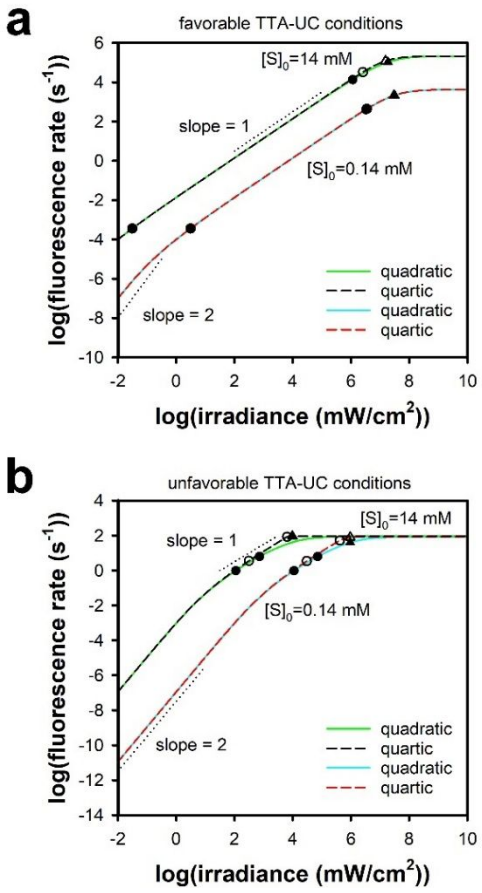

Fig. 2 Log-log plot of the fluorescence versus irradiance for the quadratic (solid lines) and quartic (dashed lines) models for solutions containing $[A]_0$ = 100 mM and $[S]_0$ = 14 mM and 0.14 mM, with k_{TTA} is fixed at (a) 3.6 × 10^8 $M^{-1}s^{-1}$ and (b) 3.6 × 10^4 $M^{-1}s^{-1}$ (see Table S1 for a list of parameters). Here, it is assumed that B_{ISC} is unity, and that the rates of ISC between $^1A^*$ and $^3A^*$ and RISC between $^3A^{**}$ and $^1A^*$ are negligibly small. The range of Γ is denoted by

circles and I_{sat} is denoted by triangles. Solid symbols represent the quadratic model and open symbols represent the quartic model. I_{th} is identical for both models for a given set of conditions. In (a) I_{th} is -0.896 for the lower value of $[S]_0$ and -2.896 for the higher value of $[S]_0$. In (b) I_{th} is 3.104 for the lower value of $[S]_0$ and 1.104 for the higher value of $[S]_0$.

Because the quadratic model is the simpler of the two, is relevant for most TTA-UC systems of interest, produces tractable and insightful analytical results, and can be used not only for modelling, but also for the fitting of data, we will focus on this model for the remainder of this paper. However, we will highlight any situations in which the quartic model might be expected to give results that are meaningfully different from those of the quadratic model.

Spin statistics

Rigorous spin-multiplicity restrictions give an excited singlet state a 1/9 statistical probability of being created via TTA. However, if quintuplet states are energetically inaccessible via TTA, then singlet excited states are generated with a 1/4 statistical probability (Fig. 1b).[16-18] A triplet excited state generated by TTA ($^3A^{**}$) can decay rapidly to the lowest triplet state ($^3A^{*}$) via internal conversion. These $^3A^{*}$ species then reenter the reaction pool. A molecule in the $^3A^{**}$ state can also undergo reverse RISC, typically to a highly excited singlet state.[19-21] To account for the probability of TTA leading to a singlet excited state, a scaling factor is included to implement spin statistics in a kinetic model.[15, 22] We consider the generation of the excited triplet state and its decay pathways explicitly, and consequently can explore how the internal conversion rate constant k_{IC} affects the upconverted fluorescence and its quantum yield. Although k_{IC} is expected to be large,[23] the density of states of highly vibrationally excited singlet states at the energy of the excited triplet state is large enough that RISC can compete with internal conversion in some cases.[21, 24]

When the rate of internal conversion dominates over the rate of RISC, the latter of which is represented by the rate constant k_{RISC}, the theoretical maximum quantum yield of the TTA process is 20%. However, this theoretical ceiling can be exceeded when k_{RISC} is large enough that the branching ratio for RISC, $\beta_{RISC} = \frac{k_{RISC}}{k_{IC} + k_{RISC}}$, is non-zero. At steady state at high enough irradiance that the quenching rate is negligible, the rate of loss of annihilator triplets via TTA plus the rate of increase of annihilator triplets though internal conversion from higher-order triplets is equal to the sum of the rates of excited singlets being created via TTA and via RISC; this equilibrium can be expressed as

$$-k_{TTA}[^3A]_{SS}^2(1.25 + 0.75\beta_{RISC}) = k_{TTA}[^3A^*]_{SS}^2(0.25 + 0.75\beta_{RISC}) \ . \quad (12)$$

The maximum theoretical quantum yield of the TTA process (i.e., assuming lossless sensitization and a unity fluorescence quantum yield) can be expressed as the number of annihilator singlets that are generated for each annihilator triplet expended:

$$\Phi_{UC,max} = \frac{0.25 + 0.75\beta_{RISC}}{1.25 + 0.75\beta_{RISC}} . \quad (13)$$

When β_{RISC} is 0, $\Phi_{UC,max}$ is 20%. On the other hand, when β_{RISC} is 1, $\Phi_{UC,max}$ is 50%. The latter case is akin to neglecting the effect of spin statistics completely. Experimentally, it is difficult to obtain a reliable estimate for the rate at which RISC takes place. Therefore, we ignore RISC below, but the effects of this process can easily be incorporated in the manner described here.

An expression for I_{th} with mass conservation included

Many of the characteristics of the TTA-UC process in our model can be understood by simplification of eqn (9). Indeed, an analysis of eqn (9) that ignores the effects of mass conservation allows us to derive an expression for I_{th}. Such an analysis is included in the ESI.

Here, we consider our complete TTA model, including mass conservation. For simplicity, we will assume that $k_{ISC}' = 0$, $B_{ISC} = 1$, and $k_{sens}[A]_{SS} \cong k_{sens}[A]_0$. Under these conditions, the complete solution of eqn (9) with conservation of mass is

$$[^3A^*]_{SS} = \frac{\alpha(k_{fl}+k_{NR})k_{IC}}{2\gamma}\left(\sqrt{1+\frac{4k_{sens}k_{ex}I[S]_0[A]_0\gamma}{\alpha^2(k_{fl}+k_{NR}^A)k_{IC}}}-1\right), \quad (14)$$

where

$$\alpha = k_T^A\left(k_{ex}I + k_{sens}[A]_0 + k_T^S\right) + k_{sens}k_{ex}I[S]_0 \quad (15)$$

and

$$\gamma = k_{TTA}\left(1.25\left(k_{ex}I + k_{sens}[A]_0 + k_T^S\right)\left(k_{fl}+k_{NR}^A\right)k_{IC} + k_{sens}k_{ex}I[S]_0\left(0.25k_{IC} + 0.75\left(k_{fl}+k_{NR}^A\right)\right)\right). \quad (16)$$

We examine eqn (14) under three different limits. If the second term in the radicand is much smaller than 1, then we find that

$$[^3A^*]_{SS} = \frac{k_{sens}k_{ex}I[S]_0[A]_0}{k_T^A\left(k_{ex}I + k_{sens}[A]_0 + k_T^S\right) + k_{sens}k_{ex}I[S]_0}. \quad (17)$$

As we are operating in the low irradiance regime, we can assume that $k_{ex}I$ is much smaller than $k_{sens}[A]_0 + k_T^S$, and that the quenching rate k_T^A is much larger than $k_{sens}k_{ex}I[S]_0$. Thus, we obtain:

$$F_{SS,low} = 0.25\Phi_{fl}k_{TTA}[^3A^*]_{SS}^2 = 0.25\Phi_{fl}k_{TTA}\left(\frac{\beta_{sens}k_{ex}I[S]_0}{k_T^A}\right)^2. \quad (18)$$

Here, β_{sens} is the branching ratio of triplet sensitization from the sensitizer, which is defined as

$$\beta_{sens} = \frac{k_{sens}[A]_0}{k_{sens}[A]_0 + k_T^S}. \quad (19)$$

As expected, the fluorescence intensity scales as I^2 in the low irradiance regime.

In the high irradiance limit, the second term in the radicand in eqn (14) is much larger than 1, so the equation reduces to

$$[^3A^*]_{SS} = \sqrt{\frac{k_{sens}k_{ex}I[S]_0[A]_0(k_{fl}+k_{NR}^A)k_{IC}}{k_{TTA}\left(1.25(k_{ex}I+k_{sens}[A]_0+k_T^S)(k_{fl}+k_{NR}^A)k_{IC}+k_{sens}k_{ex}I[S]_0(0.25k_{IC}+0.75(k_{fl}+k_{NR}^A))\right)}}\,. \quad (20)$$

With some rearrangement, this equation can be written as

$$[^3A^*]_{SS} = \sqrt{\frac{k_{sens}[S]_0[A]_0k_{ex}I}{k_{TTA}\left(1.25(k_{sens}[A]_0+k_T^S)+1.25k_{ex}I+k_{sens}[S]_0k_{ex}I\left(\frac{0.25}{k_{fl}+k_{NR}^A}+\frac{0.75}{k_{IC}}\right)\right)}}\,. \quad (21)$$

The fluorescence rate in the high irradiance limit is then

$$F_{SS,high} = \Phi_{fl}\frac{k_{sens}[S]_0[A]_0k_{ex}I}{5(k_{sens}[A]_0+k_T^S)+5k_{ex}I+k_{sens}[S]_0k_{ex}I\left(\frac{1}{k_{fl}+k_{NR}^A}+\frac{3}{k_{IC}}\right)}\,. \quad (22)$$

As long as the first term dominates the denominator, the rate of fluorescence will be linear in irradiance, which is the classic definition[9, 12, 15] of the high-irradiance regime:

$$F_{SS,high} = \Phi_{fl}\frac{\beta_{sens}[S]_0k_{ex}I}{5}\,. \quad (23)$$

We find I_{th} by setting eqn (18) equal to eqn (23) and solving for the irradiance:

$$I_{th} = \frac{k_T^{A2}}{1.25\beta_{sens}k_{ex}k_{TTA}[S]_0}\,. \quad (24)$$

Our result for I_{th} is similar to the expressions that Monguzzi *et al.*[9] and Murakami and Kamada[15] have derived, even though neither of these groups used mass conservation in their treatments. The reason for this correspondence is that in our analysis we considered a TTA-UC system that exhibits ideal characteristics, which allows us to assume that the second term in the radicand of eqn (14) is much larger than 1 at irradiances for which $k_{ex}I \ll k_{sens}[A]_0$. If this assumption does not hold, as for example when a TTA-UC system has a high rate of triplet quenching, fluorescence saturation occurs at high irradiance. Saturation would cause the region in a log-log plot with a slope of 1 to appear at lower irradiance than would be the case in the

absence of saturation. It is also possible that the region with a slope of 1 in the log-log plot could be vanishingly small due to the effects of fluorescence saturation. We therefore next consider the saturation regime.

The saturation regime

When $k_{ex}I \gg k_{sens}[A]_0$, eqn (14) becomes

$$[^3A^*]_{SS} = \frac{\alpha'(k_{fl}+k_{NR})k_{IC}}{2\gamma'}\left(\sqrt{1+\frac{4k_{sens}[S]_0[A]_0\gamma'}{\alpha'^2(k_{fl}+k_{NR}^A)k_{IC}}}-1\right), \quad (25)$$

where α' and γ' are irradiance independent versions of α and γ that are given by

$$\alpha' = k_T^A + k_{sens}[S]_0 \quad (26)$$

and

$$\gamma' = k_{TTA}\left(1.25\left(k_{fl}+k_{NR}^A\right)k_{IC} + k_{sens}[S]_0\left(0.25k_{IC}+0.75\left(k_{fl}+k_{NR}^A\right)\right)\right), \quad (27)$$

respectively. An exact solution for the rate of fluorescence at saturation can be obtained from eqn (25). However, to simplify matters, we once again assume that the second term in the radicand is much greater than 1, yielding

$$[^3A^*]_{SS} = \sqrt{\frac{k_{sens}[S]_0[A]_0}{k_{TTA}\left(1.25+k_{sens}[S]_0\left(\frac{0.75}{k_{IC}}+\frac{0.25k_{IC}}{k_{fl}+k_{NR}^A}\right)\right)}}. \quad (28)$$

The corresponding expression for the rate of fluorescence is

$$F_{SS,sat} = \Phi_{fl}\frac{k_{sens}[S]_0[A]_0}{5+k_{sens}[S]_0\left(\frac{1}{k_{fl}+k_{NR}^A}+\frac{3}{k_{IC}}\right)}. \quad (29)$$

This expression is independent of irradiance, and so increased photon flux in this regime does not result in increased light harvesting. The saturation fluorescence rate is independent of the main factors that affect I_{th} when mass conservation is not considered, such as k_{ex}, k_T^A, and k_{TTA}. Instead, $F_{SS,sat}$ depends linearly on the initial concentration of annihilators, $[A]_0$, and on k_{sens}, until the sensitization rate constant becomes large enough. This behavior is another manifestation of saturation.

We next examine the effect of k_{IC} on the saturation behavior of TTA-UC systems. In the unlikely scenario that $k_{IC} \ll k_{sens}[S]_0$, eqn (29) becomes

$$F_{SS,sat} = \Phi_{fl}\frac{k_{IC}[A]_0}{3}. \quad (30)$$

Therefore, we see that k_{IC} presents an alternate pathway to fluorescence saturation in cases in which the rate of internal conversion may be limited. In the more likely scenario that k_{IC} is large, eqn (29) becomes

$$F_{SS,sat} = \Phi_{fl}\frac{k_{sens}[S]_0[A]_0}{5 + \frac{k_{sens}[S]_0}{k_{fl}+k_{NR}^A}}. \quad (31)$$

In this limit, excited triplets decay immediately to T_1, and so are ready to undergo another TTA event. When $k_{sens}[S]_0 \gg k_{fl} + k_{NR}^A$, this expression further reduces to

$$F_{SS,sat} = \Phi_{fl}[A]_0 . \quad (32)$$

This equation represents an ideal limit in which the fluorescence rate and the annihilator concentration are the limiting factors in determining the saturation fluorescence intensity.

The saturation threshold and the efficient performance range for TTA-UC systems

Now that we have established that our model exhibits saturation, we turn to the issue of quantifying the onset of saturation. To do so, we define a quantity, I_{sat}, that is the intersection

point between tangent lines drawn on the regions of the logarithmic plot of fluorescence versus irradiance in which the slopes are 1 and 0. By setting eqn (23) equal to eqn (29) and solving for the irradiance, we find that

$$I_{sat} = \frac{5\left(k_{sens}[A]_0 + k_T^S\right)}{k_{ex}\left(5 + k_{sens}[S]_0\left(\frac{1}{k_{fl}+k_{NR}^A} + \frac{3}{k_{IC}}\right)\right)}. \quad (33)$$

This result shows that increasing $k_{sens}[A]_0$ generally delays the onset of fluorescence signal saturation, whereas increasing k_{ex} hastens the onset of fluorescence signal saturation.

Monguzzi and *et al*. proposed that the intensity of upconverted fluorescence emission saturates when $[^3A^*]_{SS}$ approaches $[A]_0$.[10] However, this conjecture does not hold strictly. The bottleneck in the growth of F_{SS} with I is the rate of sensitization. The rate of sensitization in our model is described by the quantity:

$$R_{sens} = k_{sens}[^3S^*]_{SS}[A]_{SS} = \frac{B_{ISC}k_{sens}k_{ex}I[S]_0}{B_{ISC}k_{ex}I + k_{sens}[A]_{SS} + k_T^S}[A]_{SS}. \quad (34)$$

Based on mass conservation of the annihilator, eqn (7), there are two main avenues through which F_{SS} saturates. The limited availability of annihilator ground states at high irradiance is one obvious avenue for saturation, as Monguzzi pointed out.[10] In the scenario in which k_{sens} is large, $R_{sens}\rightarrow 0$ as $[^3A^*]_{SS}\rightarrow[A]_0$, and therefore $[A]_{SS}\rightarrow 0$. However, this situation would only occur when the regeneration of ground-state annihilators is muted by slow TTA kinetics and long annihilator triplet lifetimes. Another avenue for saturation is for k_{sens} to be small. In this case, R_{sens}, and therefore F_{SS}, may saturate even when a significant portion of annihilator molecules remain in the ground state and available for triplet sensitization. Indeed, it is only possible for $[^3A^*]_{SS}$ to approach $[A_0]$ when k_{sens} is large (Fig. S2). Under such conditions, we find that $[A]_{SS} \ll [A]_0$, which necessitates the use of the quartic model. Eqn (33) describes I_{sat} under ideal conditions, in which sensitized annihilator triplets are rapidly expended through

TTA, thus allowing us to assume that $[A]_{SS} \approx [A]_0$. When this approximation is made, $[^3S^*]_{SS}$ is independent of $[A]_{SS}$. In contrast, the quartic model predicts that $[^3S^*]_{SS}$ will increase as $[A]_{SS}$ approaches zero, thus allowing the rate of fluorescence to continue to increase linearly with I until a sharp transition to saturation occurs, at a lower irradiance than in the quadratic model. The degree to which I_{sat} differs in the quartic and quadratic models is explored in Figs. S3a and S3b.

To examine and visualize the range of irradiances through which the TTA-UC system is most efficient, we define a transition width, Γ, that describes the logarithmic change in irradiance needed to bring the local slope of the logarithmic curve from 1.1 to 0.9, i.e. $\log(I_{0.9}/I_{1.1})$. The dependences of Γ on the logarithms of the quantities k_{sens}, k_{TTA}, k_T^A, $[A]_0$, and $[S]_0$ are shown in Fig. S4 for the quadratic model. The corresponding Γ values in the quartic model are generally, but not always, larger; see Fig. S3c and the ESI. All of the plots feature linear regions with a slope of 1, except that for k_T^A, which has a linear region with a slope of -2. This linear relationship generally holds when $10^6 > \Gamma > 10^{1.5}$.

Γ saturates at high values of $[S]_0$ and k_{sens}. We explore this behavior further by analyzing the related quantity $\log(I_{sat}/I_{th})$. The horizontal distances between irradiances on a log-log plot of F_{SS} vs. I that correspond to the quantities $\log(I_{sat}/I_{th})$ and Γ are highlighted in Figs. 2c and 2d. Γ is always smaller than $\log(I_{sat}/I_{th})$, by definition. The transition width Γ and $\log(I_{sat}/I_{th})$ exhibit a similar trend with respect to the parameters k_{sens}, k_{TTA}, k_T^A, $[A]_0$, and $[S]_0$. The relationships between $\log(I_{sat}/I_{th})$ and the system parameters k_{sens}, k_{TTA}, k_T^A, $[A]_0$, and $[S]_0$ in the quadratic model are shown in Fig. S5. I_{th} decreases with k_{TTA}, and increases as $(k_T^A)^2$, whereas I_{sat} is typically independent of k_{TTA} and k_T^A. Therefore, $\log(I_{sat}/I_{th})$ scales as k_{TTA} and as $(k_T^A)^{-2}$. Conversely, I_{sat} has a linear dependence on $[A]_0$, whereas I_{th} is largely

independent of $[A]_0$, assuming that $\Phi_{sens} \approx 1$. Therefore, $\log(I_{sat}/I_{th})$ scales with $[A]_0$. As is shown in Fig. S3, $\log(I_{sat}/I_{th})$ is smaller in the quartic model. However, $\log(I_{sat}/I_{th})$ depends on the parameters considered in a similar manner.

The behaviors of $\log(I_{sat}/I_{th})$ with respect to $[S]_0$ and k_{sens} are more complex. In the case of $[S]_0$, both I_{th} and I_{sat} decrease as $[S]_0$ increases. However, I_{th} decreases at a faster rate than I_{sat} when $[S]_0$ is small. Eqn (33) can be expressed as $I_{sat} = \frac{1}{X + Y[S]_0}$, where *X* and *Y* are large constants. When $[S]_0$ is large, $Y[S]_0$ becomes much larger than *X*, and so I_{sat} decreases at approximately the same rate that I_{th} decreases, which causes $\log(I_{sat}/I_{th})$ to become independent of $[S]_0$. The value of $\log(I_{sat}/I_{th})$ also reaches an asymptote when k_{sens} is large enough, such that both I_{th} and I_{sat} become independent of this rate constant.

In Figs. S4c and S4e, k_T^A was set to 2.0×10^4 s^{-1} instead of 2.0×10^2 s^{-1}, the latter of which was the value used in the remaining panels in this figure. Fig. S6 shows the behavior of the transition width when $k_T^A = 2.0 \times 10^2$ s^{-1}. In this case, the dependence of Γ on both k_{TTA} and $[A]_0$ has an exponent of ~1.6, rather than an exponent of unity. This behavior is explained further in the ESI.

The local slope of logarithmic plots of F_{ss} vs. *I*.

We note that the local slope of a logarithmic plot of F_{SS} vs. *I* is an important property in the study of TTA-UC, because this slope allows for the description of the relationship between F_{SS} and *I* succinctly at any irradiance. The irradiance dependent local slope, which we denote *n*(*I*), may be expressed as:

$$\frac{d(\log(F_{ss}))}{d(\log(I))} = \frac{I}{F_{ss}} \cdot \frac{dF_{ss}}{dI}. \quad (35)$$

A thorough analysis of eqn (35) is presented in the ESI.

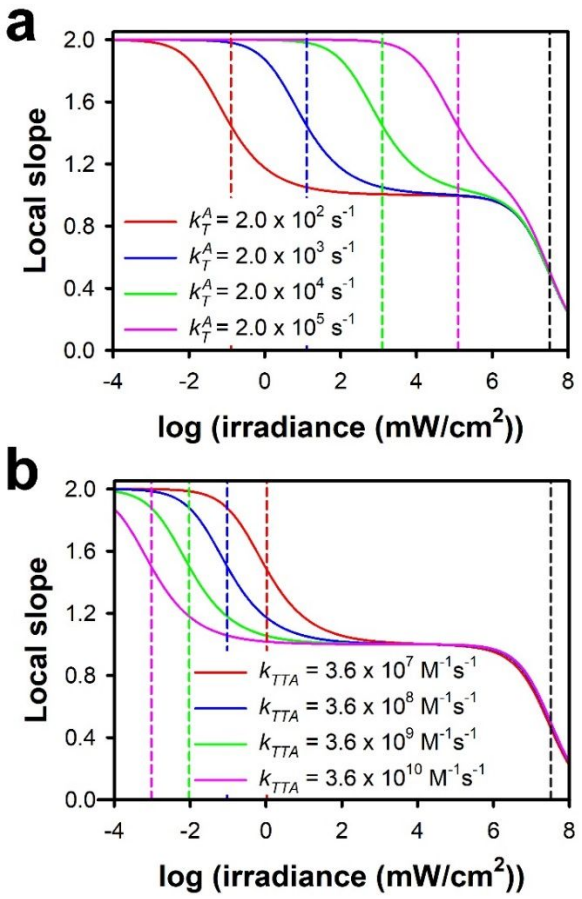

Fig. 3 Dependence of the local slope $n(I)$ on the irradiance I for different values of (a) k_T^A and (b) k_{TTA}. See Table S1 for the values of the other parameters. The colored dashed lines indicate the irradiance at which $n = 1.5$ for the curve of the corresponding color, and the black dashed lines indicate the irradiance at which $n = 0.5$.

From eqn (35), we find that for any TTA-UC system, $n(I)$ is close to 2 at low irradiances. As I increases beyond I_{th}, F_{ss} begins to scale linearly with I, and so $n(I)$ approaches a value of 1. We note that if mass conservation is not considered, $n(I)$ never reaches a value of 1. However, in our model, the quantity $k_{sens}[A]_0$ limits the increase of F_{SS} at high irradiances, allowing $n(I)$ to attain a value of 1. When $I > I_{sat}$, F_{ss} begins to saturate. Therefore, at high enough irradiance, $n(I)$ approaches 0. Figures 3a and 3b show characteristic plots of $n(I)$ as a function of I for different values of k_T^A and k_{TTA}, respectively. The value of n is roughly 2 at

low irradiance, and declines rapidly as I approaches the quantity $\frac{4(k_T^A)^2}{5k_{TTA}k_{ex}[S]_0}$, which is an approximate expression for I_{th}. There is another sharp decline in $n(I)$ that persists until I approaches the quantity $\frac{k_{sens}[A]_0}{k_{ex}}$, which is an approximate expression for I_{sat}. For a typical TTA-UC system, the quantities $\frac{4(k_T^A)^2}{5k_{TTA}k_{ex}[S]_0}$ and $\frac{k_{sens}[A]_0}{k_{ex}}$ are of different enough magnitudes that there is an extended range of irradiances for which the local slope is close to 1. However, for some TTA-UC systems, the two aforementioned quantities may lie close to one another, which can make the portion of the log-log plot that possesses a slope of 1 vanishingly small.

The points at which $n(I)$ attains a value of 1.5 ($I_{1.5}$) and a value of 0.5 ($I_{0.5}$) are analogues to I_{th} and I_{sat}, respectively. Figure 4a shows that $I_{1.5}$ initially scales as $\left(k_T^A\right)^2$, but reaches an asymptote as k_T^A exceeds 10^6 s^{-1}. This behavior stems from the fact that when k_T^A becomes large enough, the value of $\frac{4(k_T^A)^2}{5k_{TTA}k_{ex}[S]_0}$ approaches the value of $\frac{k_{sens}[A]_0}{k_{ex}}$. Indeed when $\frac{4(k_T^A)^2}{5k_{TTA}k_{ex}[S]_0} \gg \frac{k_{sens}[A]_0}{k_{ex}}$, $I_{1.5}$ is completely independent of k_T^A, and is determined primarily by $\frac{k_{sens}[A]_0}{k_{ex}}$. Similarly, if k_{sens} is small, the condition $\frac{4(k_T^A)^2}{5k_{TTA}k_{ex}[S]_0} \gg \frac{k_{sens}[A]_0}{k_{ex}}$ is once again satisfied, and $I_{1.5}$ becomes strongly dependent on the term $\frac{k_{sens}[A]_0}{k_{ex}}$. Therefore, the decline in $n(I)$ under non-ideal TTA-UC conditions is a consequence of fluorescence saturation, rather than an indication that the TTA process has become efficient. Figure 4b illustrates the source of this behavior. When we compare the dependence of $n(I)$ on I for substantially different values of k_{sens}, we see that both curves overlap when $n(I)$ is close to 2. As all rate constants except k_{sens} are held constant in these curves, one might expect that the declines in $n(I)$ from a value of 2 to a value of 1 would be identical. However, Fig. 4b shows that $n(I)$ decreases more quickly when k_{sens} is small, because $n(I)$ undergoes an earlier descent towards a value of 0 due to the saturation of $[^3S^*]_{SS}$, and consequently $[^3A^*]_{SS}$. Because the dependence of $n(I)$ on I must be smooth and continuous

for all values of I, the value of I at which n attains a value of 1 must decrease when k_{sens} decreases. The significance of this finding is that it is not desirable for a TTA-UC system to possess a small I_{th} if this value is a consequence of an early onset of saturation.

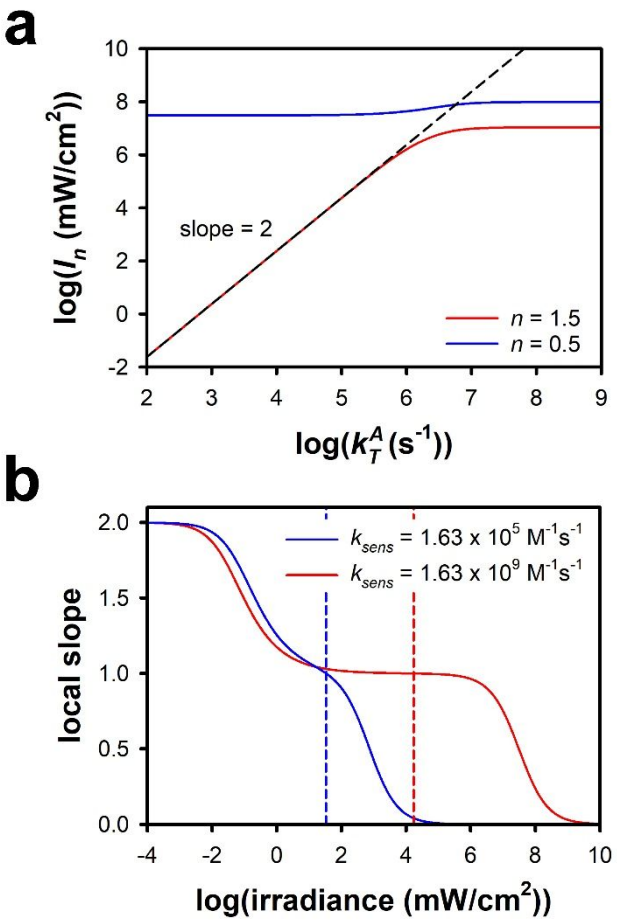

Fig. 4 (a) Dependence of $I_{1.5}$ (red) and $I_{0.5}$ (blue) on k_T^A. (b) The local slope as a function of irradiance for a small sensitization rate constant (blue) and a typical sensitization rate constant (red). The dashed lines indicate the point at which n = 1 in the corresponding curve. See Table S1 for the values of the other parameters.

Visualizing the change in upconverted fluorescence intensity across a range of irradiance

We saw above that in the low irradiance limit, the rate of excitation is small, such that the second term in the radicand in eqn (14) must be much less than 1. Assuming that we are far

away from the saturation region, i.e. that $k_{sens}[A]_0 \gg k_{ex}I$, the second term in the radicand being small implies that

$$\frac{k_T^A[A]_0}{5k_{TTA}[A]_0^2} \gg \frac{k_{ex}I[S]_0}{k_T^A[A]_0}. \quad (36)$$

In an ideal TTA-UC system, in which $k_{TTA} \gg k_T^A$, the irradiance has to be small for the system to remain in the quadratic regime by satisfying the condition that $k_{ex}I[S]_0 \ll k_T^A[A]_0$. On the other hand, for a non-ideal TTA-UC system, in which either k_T^A is large or k_{TTA} is small, the quadratic irradiance regime can extend over a larger range. As shown in Figs. 5a and 5b, as k_T^A increases, so does the maximum irradiance at which the local slope is 2. Conversely, as shown in Figs. 5c and 5d, the maximum irradiance at which the local slope is 2 decreases with increasing k_{TTA}. In the high irradiance limit, $\frac{k_T^A[A]_0}{5k_{TTA}[A]_0^2} \ll \frac{k_{ex}I[S]_0}{k_T^A[A]_0}$. This inequality is equivalent to $I \gg \frac{(k_T^A)^2}{5k_{TTA}k_{ex}[S]_0}$, which implies that the local slope approaches 1 at smaller irradiance values when k_T^A is small and k_{TTA} is large (cf. Figs. 5b and 5d.)

Next, we consider the saturation regime, in which $k_{ex}I > k_{sens}[A]_0$. When either k_{sens}, $[A]_0$, or both, are high enough, a large irradiance is required for saturation to be observed, as shown in Fig. S7. The rate constants k_{TTA} and k_T^A have little effect on the signal saturation, and may be factored out of the equation for F_{ss} in most instances. Figure 5 shows that TTA-UC systems with different k_{TTA} and k_T^A values exhibit saturation at identical values of *I*. In implementing mass conservation, we consider $[A]_0$ to be an emitter species "reservoir" that is consumed as the irradiance increases. Although the emission intensity does not scale proportionally with $[A]_0$ along the entire log-log plot, the maximum achievable emission intensity does scale with $[A]_0$. Figures S7a and S7b show that increasing $[S]_0$ and $[A]_0$ concurrently extends the region in which $n(I) \sim 1$ in both directions. Figures S7c and S7d demonstrate that an increase in k_{sens}

results in a proportional extension of the region in which $n(I) \sim 1$ towards higher I. The effect of k_{sens} on signal saturation can be understood based on the fact that the TTA-UC process, under the quadratic model, can only proceed as fast as $k_{sens}[A]_0$, regardless of how quickly triplet states may be generated in the sensitizer or how quickly annihilator triplets may undergo TTA to produce fluorescent singlets.

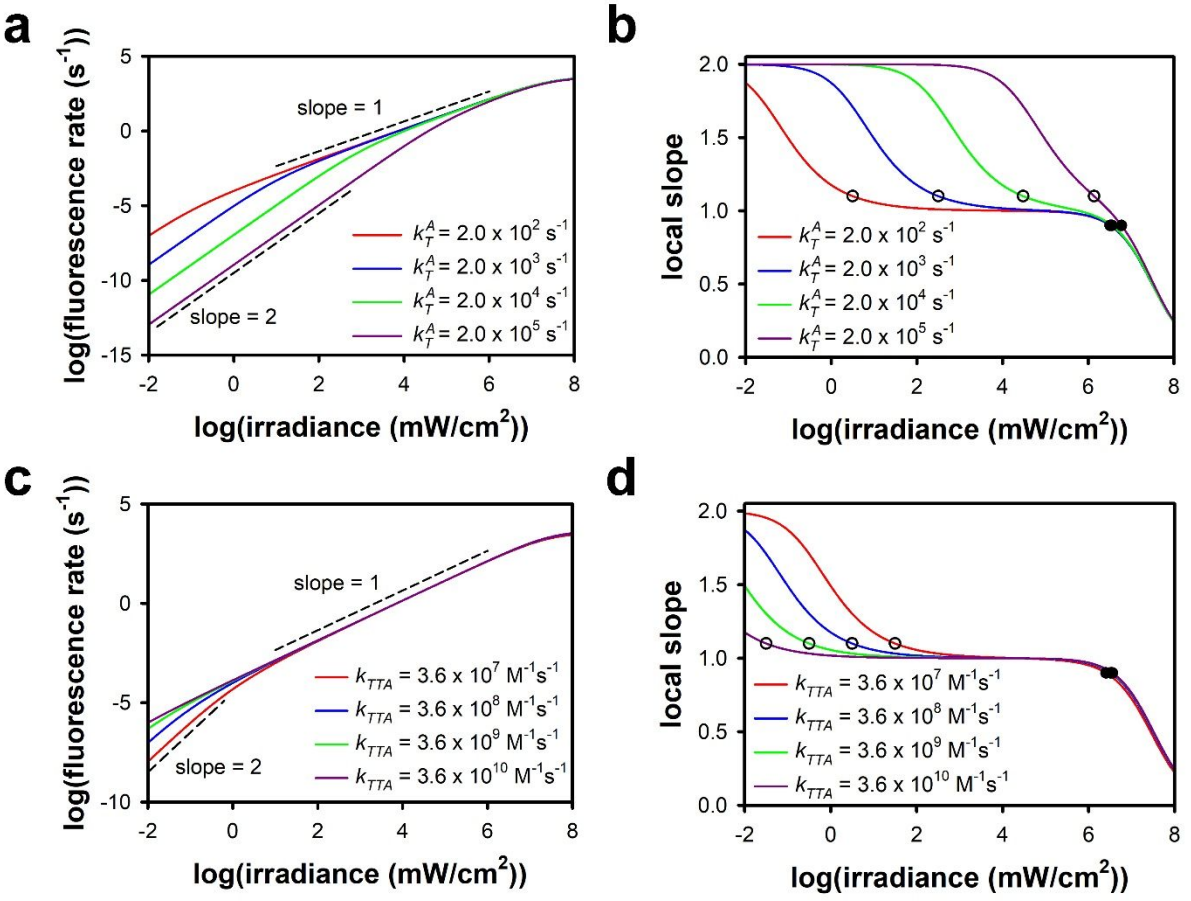

Fig. 5 Dependence of the fluorescence rate and the local slope, $n(I)$, respectively, on (a), (b) k_T^A and (c), (d) k_{TTA}. See Table S1 for the values of the other parameters. The open and filled circles indicate the irradiances at which the local slope is 1.1 and 0.9, respectively.

The TTA-UC quantum yield (Φ_{UC})

Achieving a high Φ_{UC} at low irradiance is one of the ultimate performance goals of any TTA-UC system. Φ_{UC} is the ratio of the rate of emission (F_{ss}) to the rate of absorption by the

sensitizer ($k_{ex}I[S]_{SS}$), neglecting any losses arising from an output coupling that is less than unity.[25] Because F_{SS} is proportional to $I^{n(I)}$, we can conclude that $\Phi_{UC}(I)$ must be proportional to $I^{n(I)-1}$. Therefore, at irradiances low enough that $n(I) \sim 2$, Φ_{UC} increases linearly with I. When $2 > n(I) > 1$, Φ_{UC} increases more slowly with increasing irradiance. When $n(I)$ is unity, $\Phi_{UC} \propto I^0$. The TTA-UC quantum yield reaches its maximum value at this irradiance, and decreases at higher irradiances. Thus, for any TTA-UC system, peak performance is achieved when the relationship between F_{ss} and I becomes strictly linear. As $n(I)$ approaches 0, Φ_{UC} becomes inversely proportional to I. As a result, Φ_{UC} decreases at irradiances high enough to saturate the intensity of upconverted fluorescence. This behavior is illustrated in Fig. 6 for different values of k_T^A (Figs. 6a, 6b) and k_{TTA} (Figs. 6c and 6d). As shown in Figs. 6b and 6d, the slope of the quantum yield for the data in Figs. 6a and 6c undergoes a smooth transition from a value of 1 at low irradiance, to a value of 0 when $n(I) = 1$, and then finally to a value of -1 at high irradiance.

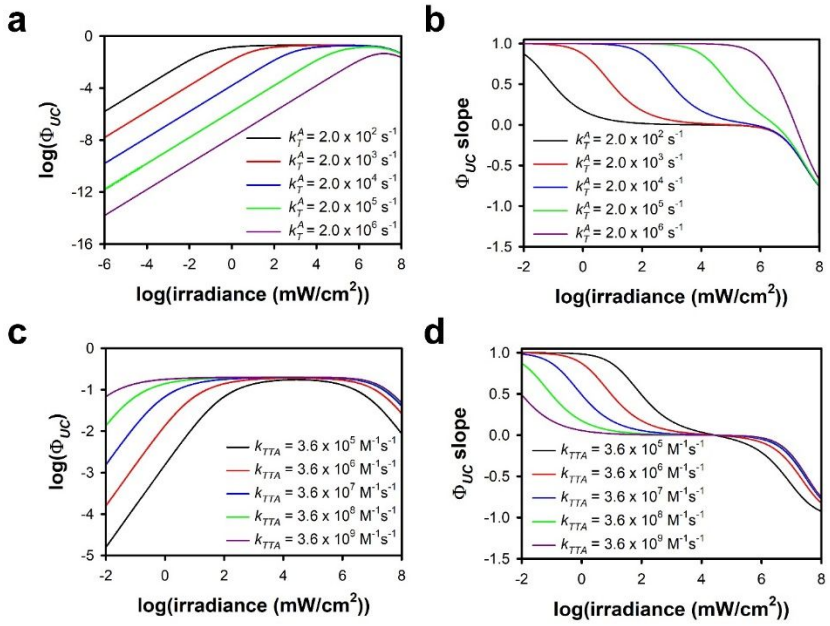

Fig. 6 The dependence of the upconversion quantum yield and its slope on irradiance for (a) and (b), respectively, different values of k_T^A, and (c) and (d), respectively, different values of k_{TTA}. See Table S1 for the values of the other parameters.

We next consider the relationship between $\Phi_{UC}(I)$ and $n(I)$. Fig. S8 shows that for an ideal TTA-UC system, Φ_{UC} increases monotonically as $n(I)$ decreases from a value of 2 to a value of 1. In this case, we find empirically that the relationship between $\Phi_{UC}(I)$ and $n(I)$, when $1 \leq n(I) \leq 2$, is described by an equation of the form

$$\Phi_{UC}(I) \propto ae^{-b \cdot n(I)} + c\,, \tag{37}$$

where, a, b and c are positive constants (Fig. S9). When k_T^A is small and k_{TTA} is large, Φ_{UC} can be estimated reliably given knowledge of $n(I)$. However, as k_T^A becomes larger and k_{TTA} becomes smaller, the relationship between Φ_{UC} and $n(I)$ deviates significantly from that in eqn (37). Furthermore, the highest achievable TTA-UC quantum yield ($\Phi_{UC,\,max}$) decreases as k_T^A increases and k_{TTA} decreases. We also define the TTA-UC quantum yield fraction ($\overline{\Phi}_{UC}$) as

$$\overline{\Phi}_{UC} = \frac{\Phi_{UC}}{\Phi_{UC,\,max}}\,. \tag{38}$$

$\overline{\Phi}_{UC}$ reaches a peak value of 1 when a TTA-UC system achieves its maximum possible Φ_{UC}. $\overline{\Phi}_{UC}$ increases towards a value of 1 steeply as $n(I)$ approaches 1, as highlighted in Fig. S8. Under non-ideal TTA-UC conditions, the dependence of $\overline{\Phi}_{UC}$ on $n(I)$ becomes steeper than in the ideal case at larger values of $n(I)$ and shallower as $n(I)$ approaches 1. This behavior is due to the influence of saturation on the value of $n(I)$.

It is typically assumed in the literature that $\Phi_{UC,\,max}$ does not depend upon k_T^A or k_{TTA}. The independence of $\Phi_{UC,\,max}$ from these rate constants only holds when one makes the assumptions that the relationship between F_{ss} and I becomes strictly linear only as $I \rightarrow \infty$, and that $F_{ss}(\infty)$ is completely independent of k_T^A and $k_{TT}[A]_{SS}$. When mass conservation is considered, k_T^A and k_{TTA} both affect the finite value of I at which the relationship between F_{ss} and I becomes strictly linear, as well as the value of F_{ss} at this point. We discussed above the requirement in ideal TTA-UC systems that the second term within the radicand in eqn (14), called ρ for convenience, be much greater than 1 at irradiances at which saturation could be avoided. Under these conditions, k_T^A and k_{TTA} may be factored out of the expression for $F_{SS,high}$, and so will not influence $\Phi_{UC,\,max}$ or $\frac{F_{SS,high}}{k_{ex}I[S]_{SS}}$. An ideal TTA-UC system attains a peak value of ρ at lower irradiance than do non-ideal TTA-UC systems (Fig. S10). For non-ideal TTA-UC systems, the rate constants k_T^A and k_{TTA} retain a strong influence on $\Phi_{UC,\,max}$. This dependence fades as $k_T^A \rightarrow 0$ and $k_{TTA} \rightarrow \infty$.

An idealized expression for $\Phi_{UC,\,max}$ takes the form

$$\Phi_{UC,\,max} = \frac{\Phi_{fl} B_{sens}[A]_0}{5[A]_0 + B_{sens} k_{ex} I[S]_0 \left[\frac{1}{3\left(k_{fl} + k_{NR}^A\right)} + \frac{1}{k_{IC}}\right]} . \tag{39}$$

Here, B_{sens} is an intensity dependent version of the branching ratio β_{sens} that is given by

$$B_{sens} = \frac{k_{sens}[A]_0}{k_{ex} I + k_{sens}[A]_0 + k_T^S} . \tag{40}$$

The second term in the denominator of eqn (39) is small when compared to the initial concentration of the annihilator, and so we arrive at an expression for the theoretical maximum quantum yield of a TTA-UC system:

$$\Phi_{UC,\,max} = 0.2\Phi_{fl}\mathrm{B}_{sens} \quad . \tag{41}$$

For such an idealized system, the maximum attainable quantum yield is limited only by the sensitization efficiency, the fluorescence quantum yield, and a scaling factor of 0.2 that arises from the implementation of spin statistics, assuming inaccessible quintets.

Fig. S11a shows that $\Phi_{UC,\,max}$ increases with k_{sens}, as predicted by eqn (39). However, when k_{sens} becomes large enough, this rate constant no longer has an effect on $\Phi_{UC,\,max}$, because there is little room to improve $\Phi_{UC,\,max}$ once B_{sens} approaches unity. The dependence of $\Phi_{UC,\,max}$ on k_T^A is particularly evident when k_T^A is large. For a representative TTA-UC system with a k_T^A of 2.0×10^2 s^{-1}, a k_{TTA} of 3.6×10^9 M^{-1} s^{-1}, and a Φ_{fl} of 0.997, $\Phi_{UC,max}$ reaches 99.5% of the theoretical maximum value at a k_{sens} value of 1.63×10^9 M^{-1} s^{-1}. When k_T^A is increased to 2.0×10^4 s^{-1} while keeping the other parameters unchanged, $\Phi_{UC,\,max}$ drops to 96.6% of the theoretical maximum value. When k_T^A is increased further to 2.0×10^6 s^{-1}, $\Phi_{UC,\,max}$ plummets to just over 51% of the theoretical maximum. We also note that at k_T^A values of 2.0×10^6 s^{-1} or 2.0×10^8 s^{-1}, $\Phi_{UC,\,max}$ remains close to 0 at low irradiances, because when k_T^A is large, ρ is small unless $k_{ex}I[S]_0$ is also large. Therefore, to drive the TTA process efficiently, we require that k_{sens} be large enough that the condition $k_{sens}[A]_0 \gg k_{ex}I[S]_0$ is satisfied.

The effect of k_{IC} on $\Phi_{UC,\,max}$ is explored in Fig. S11b. The rate constant k_{IC} governs the rate at which higher-order annihilator triplets that are formed via TTA decay back to the $^3A^*$ state, such that these triplets may participate in the TTA process once again. As $k_{IC} \rightarrow 0$, the theoretical maximum yield of singlets from the TTA process is 12.5%, because on average

only one singlet is generated for every eight triplets consumed. As $k_{IC} \rightarrow \infty$, the theoretical maximum yield of singlets increases to 20%, because the overall consumption of triplets is reduced to 5. Finally, we explore Murakami and Kamada's finding that at I_{th}, $\overline{\Phi}_{UC}$ has a value of 38.2%, whereas at an irradiance that is twice as large as I_{th}, $\overline{\Phi}_{UC}$ has a value of 50%. These findings also hold true only under ideal TTA-UC conditions, as we demonstrate in Fig. S12. In this figure, we show that $\overline{\Phi}_{UC}$ at the critical irradiance values of I_{th} and $2I_{th}$ deviates significantly from the ideal values of 38.2% and 50% under non-ideal TTA-UC conditions, specifically due to the effects of mass conservation.

The challenge of determining I_{th} experimentally

Although there is no special physical significance to I_{th}, from a practical standpoint this quantity has been an important metric for assessing TTA-UC systems. Furthermore, the value of I_{th} is often used to extract k_{TTA} when k_T^A and k_{ex} are known. To determine I_{th} reliably, one needs to obtain fluorescence measurements at low enough irradiances that a tangential line with a slope of 2 may be drawn. As discussed above, the value of $n(I)$ is 2 only at irradiances that are substantially less than I_{th}. It is not easily possible to make experimental measurements in this irradiance regime, particularly for efficient TTA-UC systems. It is also necessary to perform fluorescence measurements at high enough irradiances to attain a slope of 1. Thus, a large dynamic range is required to determine I_{th} accurately. For instance, in the example shown in Fig. 7, the dynamic range of emission intensity needed to capture the transition of a typical TTA-UC system from the quadratic to the linear regime is more than 6 orders of magnitude.

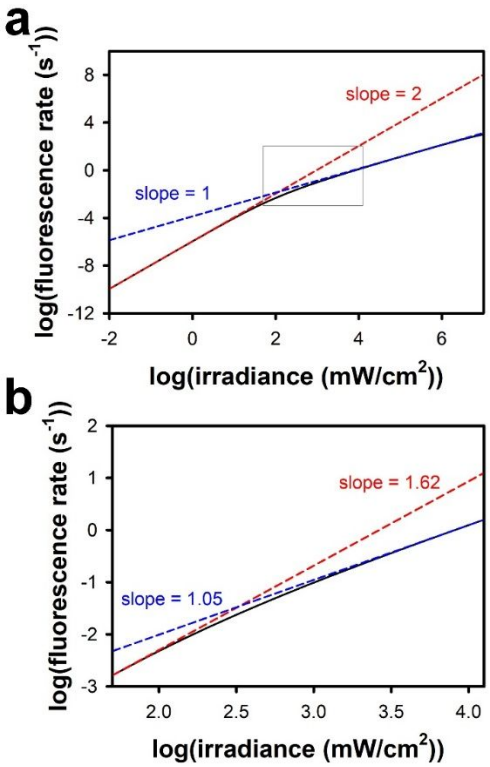

Fig. 7 TTA-UC log-log plots based on the quadratic model. (a) Capturing the quadratic and linear regions of the plot to determine I_{th} accurately requires obtaining data over 6 or more orders of magnitude in irradiance. (b) When a more typical experimental range of irradiances is used for the same data (box in (a)), the slopes do not reach 2 and 1. See Table S1 for the values of the parameters.

Experimentally, it is challenging to achieve a dynamic range of emission intensity exceeding 5 orders of magnitude. As shown in Fig. 7b, an asymmetric limitation on the local slope within the window, e.g., a maximum possible slope of 1.62 instead of 2 and a minimum slope of 1.05 instead of 1, can lead to uncertainty in the determination of I_{th}.

In Fig. S13a we show TTA-UC curves calculated with our model for three different values of k_T^A, viewed through a window that is intended to simulate experimental conditions. We show the values of I_{th} for two of these curves. The I_{th} value for the system with $k_T^A = 2.0 \times 10^4$ s^{-1} lies

beyond the range of our selected window, and therefore is not shown. For an accurate graphical interpretation of I_{th} to be made, the actual value of I_{th} must lie close to the center of the experimental window. As a measure of the difference between the visually extracted ($I_{th,graphical}$) and fit values ($I_{th,computed}$) of I_{th}, we define $\delta_I = \frac{I_{th,computed} - I_{th,graphical}}{I_{th,computed}} \cdot 100\%$. Bar plots of δ_I as function of various system parameters are shown in Fig. S13b-S13e. Using Fig. 7 as an example, at low k_T^A, the actual value of I_{th} can only be found at low values of *I*. Hence, extracting I_{th} graphically from a small experimental window (a window identical to that in Fig. 7 was used), leads to substantial overestimation of I_{th}. As k_T^A increases, the actual values of I_{th} fall closer to center of the experimental window, and thus the predicted error is minimized when $k_T^A = 2.0 \times 10^3$ s^{-1}. As k_T^A increases even further, the actual value of I_{th} can only be found at an irradiance beyond the upper limit of the experimental window. In this situation, graphically extracted values of I_{th} are underestimated. A similar trend in δ_I with respect to the parameters k_{TTA} and $[S]_0$ is shown in Figs. S13c and S13d. Because $[A]_0$ has negligible impact on I_{th}, there is little change in the predicted error with different values of $[A]_0$.

It is more reliable to estimate I_{th} from measurements of the local slope *n*(*I*). Numerical analysis of eqn (35) reveals that for a broad range of different TTA-UC systems with varying system parameters, $n(I_{th})$ takes on a value near 1.4472, in basic agreement with the findings of Murakami and Kamada using a model that did not conserve mass.[15] However, we do find that $n(I_{th})$ is not a constant, and to measure its variation from its ideal value we define $\delta_n = \frac{1.4472 - n(I_{th})}{n(I_{th})} \cdot 100\%$. As shown in Figs. S13b-S13e, δ_n in vanishingly small for a broad range of k_{sens}, k_{TTA}, $[A]_0$, and $[S]_0$, and only becomes substantial under the conditions explored when k_T^A is large.

Fitting experimental data from literature with the quadratic TTA model

Edhborg *et al*. recently outlined an approach for obtaining I_{th} by determining the fraction of annihilator triplets that decay initially through TTA (β).[26] Their approach necessitates the collection of upconverted emission decay curves to determine β for a particular value of excitation irradiance. This process is repeated for a variety of irradiances to construct a plot of β vs. *I*. This plot can then be fit analytically to obtain I_{th}, which lies at the value of *I* for which $\beta = 0.5$. Any errors arising from poor fits to the emission decay data will be compounded, potentially leading to a large uncertainty in determining I_{th}.

A more practical approach to determine I_{th} might be to fit experimental upconverted fluorescence intensity data with the full expression for F_{ss} from eqn (8), and then to obtain I_{th} from the extracted fitting parameters, k_T^A, k_{sens}, k_{TTA}, k_{ex}, k_{fl}, k_{NR}^A, and the two known quantities $[A]_0$, and $[S]_0$. Fitting is an attractive strategy for finding I_{th}, because all data points contribute to the determination of the value of this parameter, not just those at low and high irradiance. As an example, we fitted experimental data on upconverted fluorescence from a solution of 0.05 mM PtOEP and 1 mM DPA in toluene, the results of which are presented in Fig. 8a. The fit yielded an R^2 value of 0.9997. Based on the fit, I_{th} has a value of 116.5 mW/cm^2, which is little less than twice the value of 74.2 mW/cm^2 determined from the intersection point between tangential lines that were drawn over the data.

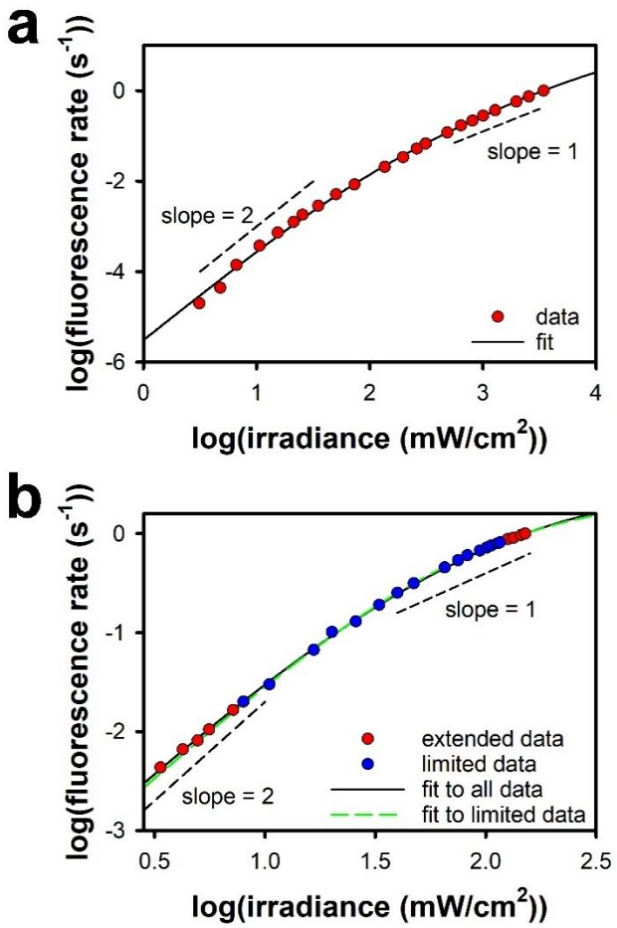

Fig. 8 Fits (solid lines) to experimental TTA-UC emission versus irradiance data (symbols) using the quadratic model. The data in (a) were collected for this paper and the data in (b) are from Deng *et al.*[27] In (b), the solid black line is a fit to all of the data, and the dashed green line is a fit to only the blue data points. See Table S1 for the values of the parameters.

Because our TTA model predicts saturation at high irradiances, we can fit data that hint at fluorescence saturation. For example, in fitting upconverted fluorescence data by Deng *et al.* from Pt(II) tetraphenyltetrabenzoporphyrin sensitized boron dipyrromethene systems, we found that our model fit conformed well to the entirety of the authors' original data, including the regions in which clear deviations from linearity are observed at high irradiance.[27] Furthermore, it is possible to use our model to fit upconverted fluorescence data over a limited

range of irradiance to extract reliable information that may aid in predicting the behavior of the TTA-UC process beyond the experimental window. In Fig. 8b we show that it is possible to obtain comparable fits both to the original data of Deng *et al*. and to a truncated version in which only upconverted fluorescence data points for irradiances between ~1 and ~100 mW/cm^2 were considered.

It is important to note that although the kinetic parameters obtained from best fits to experimental TTA-UC data may not be unique, performance metrics such as I_{th} or the theoretical quantum yield Φ_{UC} obtained by this fitting method are accurate. The system studied by Deng *et al*. appeared to lack of an extended region in the log-log plot in which the slope remained at ~1, which means that theoretically determined values of I_{th} from fitted parameter values would not be meaningful. Therefore, rather than comparing I_{th} values from the complete and truncated fits, we instead compare the points at which the local slope is expected to attain a value of 1 (I_1). I_1 values of 84.3 mW/cm^2 and 87.9 mW/cm^2 were obtained from parameters extracted from the complete and truncated fits, respectively, demonstrating that this fitting method works well even when the dynamic range of the experimental data is limited.

We were able to make robust fits to upconverted fluorescence data from a broad sampling of literature data (Figs. S14 and S15).[11, 12, 28-32] These fits enabled us to calculate δ_I using the values of I_{th} that were quoted by the authors (Fig. S16). Moreover, our model is able to fit upconversion data from non-solution-based TTA-UC systems, such as dispersed sensitizer/annihilator assemblies,[33] spin-coated TTA-UC thin films,[34, 35] metal-ion-linked sensitizer/annihilator multilayers,[36] perovskite-sensitized annihilator/acceptor solid films,[37] nanocrystal-sensitized upconversion systems,[38] and upconverting core/shell nanoparticles[39, 40] (Figs. S17-S19). The only literature systems we examined for which our model could not fit the TTA-UC data were gels[41, 42] (Fig. S20), and TTA-UC devices.[43-45] To apply our model to

TTA-UC systems in gels, we believe that adjustments would have to be made to account for additional processes, such as oxygen quenching and singlet fission within the gel pores. Modelling the complex relationship between photogenerated current from a TTA-UC device and irradiance would require careful consideration of factors such as electron injection, charge regeneration effects, and exciton loss due to recombination events in trap states.

Alternatives to I_{th} as a metric for TTA-UC systems

As we have seen, an early onset of saturation could belie the true performance of a TTA-UC system. In fact, I_{th} becomes meaningless when a system experiences an onset of saturation well before TTA becomes efficient. Therefore, I_{th} should not be relied upon as the sole metric to judge the performances of TTA-UC systems. The ratio $\psi = \frac{\log(I_{th})}{\log(I_{sat}) - \log(I_{th})}$ is an alternative means of characterizing the potential of a TTA-UC system. For an ideal TTA-UC system, log (I_{th}) should be as small as possible, whereas $\log(I_{sat}/I_{th})$ should be large, such that $\psi \ll 1$. The reverse is true for a non-ideal system.

Another alternative is the ratio $\xi = \frac{I_{th}}{I_{cr}}$, where I_{cr}, the critical irradiance, is the irradiance at which the expression for $F_{ss,low}$, eqn (18), is equal to the expression for $F_{ss,sat}$, eqn (31):

$$I_{cr} = \frac{k_T^A}{k_{ex}} \sqrt{\frac{k_{sens}[A]_0(k_{fl} + k_{NR}^A)}{k_{TTA}[S]_0(1.25(k_{fl} + k_{NR}^A) + k_{sens}[S]_0)}} \quad . \tag{42}$$

Here for simplicity, we have assumed that $k_{IC} \gg k_{sens}[S]_0$. I_{cr} is a balance among all the parameters that govern the TTA process. The critical irradiance decreases as k_{ex}, k_{TTA}, $[S]_0$, and k_T^A increase, but increases when k_{sens} and $[A]_0$ increase. The ratio ξ can be expressed as

$$\xi = k_T^A \sqrt{\frac{(k_{fl} + k_{NR}^A) + k_{sens}[S]_0}{1.25 k_{TTA}[S]_0 k_{sens}[A]_0(k_{fl} + k_{NR}^A)}}. \tag{43}$$

This ratio decreases when any of the parameters k_{ex}, k_{TTA}, $[S]_0$, k_{sens}, $[A]_0$, increases, and when k_T^A decreases. Hence, we desire ξ to be as small as possible.

We explored the applicability of these proposed metrics to TTA-UC systems from literature. We began by fitting the experimental data with our quadratic TTA model. We then used the fit to determine I_{th}, log (I_{sat}/I_{th}), and I_{cr}. In Figs. 9a-9d, we compare the performance of six experimental TTA-UC systems from literature in terms of their ψ, ξ, and I_{th} values, respectively, in addition to the projected TTA-UC quantum yield.

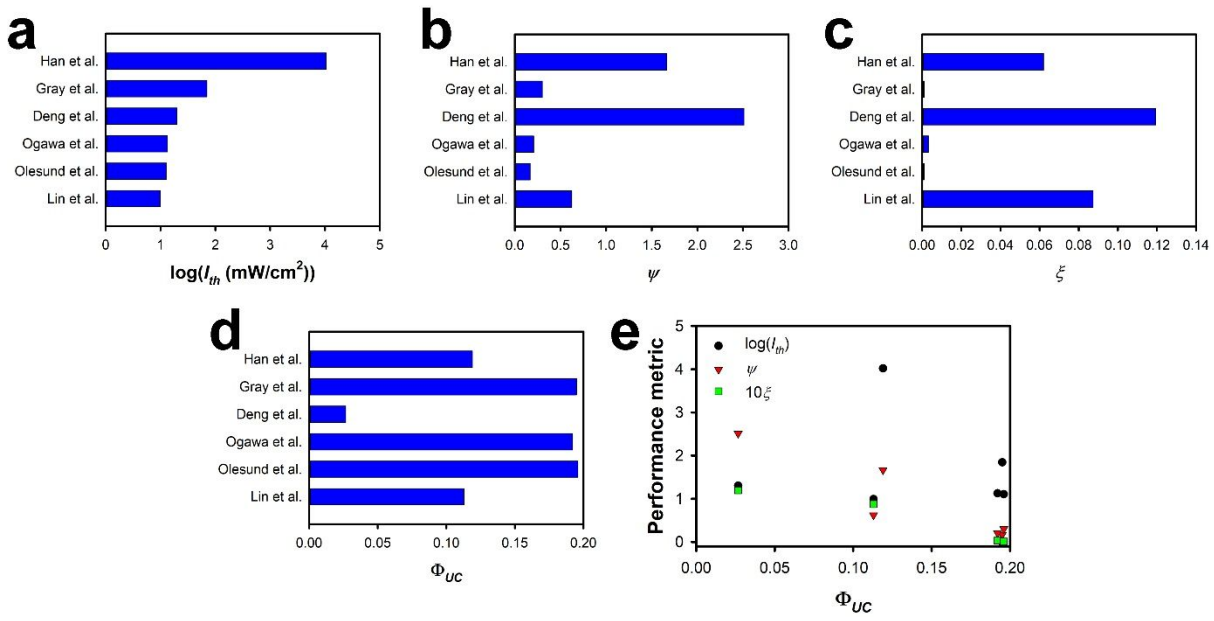

Fig. 9 Comparison of the metrics (a) I_{th}, (b) ψ, (c) ξ, and (d) Φ_{UC} for six different TTA-UC systems from the literature,[11, 27, 28, 30, 32, 35] as well as (e) a comparison of the first three metrics to Φ_{UC}.

Some of our findings were surprising. For instance, although the extracted values of I_{th} from Ogawa *et al.*,[11] Deng *et al.*,[27] and Olesund *et al.*,[28] were similar (~10 – 15 mW/cm^2), the values of ψ and ξ that were obtained from their data are quite different. The PtOEP/DPA mixture that was studied by Olesund *et al.*[28] exhibited the best performance, with ψ and ξ

values of 0.1673 and 0.00087, respectively. The self-assembled TTA-UC system that was studied by Ogawa *et al*.[11] had a poorer performance, as evidenced by a reduced analytical transition width, log (I_{sat}/I_{th}). A ψ value of 0.2065 and a ξ value of 0.0032 were determined from their data. Respective values of ψ and ξ of 2.512 and 0.3920 were obtained by analyzing upconverted fluorescence data from Deng *et al*.[27] When we analyzed an earlier work on TTA-UC emission from Gray *et al*.[32], we found that their system possessed a relatively large I_{th} (~70 mW/cm^2). However, their system also exhibited low ψ and ξ values (0.3010 and 0.00088, respectively). Lin *et al*.[35] studied TTA-UC from mixtures of diiodo-BODIPY and perylene. Their system exhibited an extraordinarily low I_{th} of 8.9 mW/cm^2, although the data exhibited an early onset of saturation. We found high ψ and ξ values of 0.6225 and 0.1194, respectively, from fits performed on their data.

One key aspect of a good performance metric is a strong correlation with Φ_{UC}. Accordingly, in Fig. 9e we plot each of the performance metrics versus Φ_{UC}. For consistency, the quantum yield was determined from the best fit to each of the 6 sets of literature data with our TTA model. Neither log(I_{th}) nor ψ is correlated strongly with Φ_{UC}, although there is a rough trend for ψ to decrease with increasing Φ_{UC}. Therefore, neither of these metrics is a good predictor of Φ_{UC}. On the other hand, ξ decreases with increasing quantum yield, and so may be a good proxy for Φ_{UC}. From a different standpoint, ψ is an excellent complementary metric to ξ considering that a TTA-UC system's upconversion quantum yield and its ability to perform efficiently at low excitation powers are both important.

Conclusions and future outlook

We have developed a mass-conserving TTA model that is able to describe TTA-UC behaviour over all irradiance regimes. An important consequence of including mass conservation is that

the upconverted fluorescence intensity saturates once the rate of excitation exceeds the rate of triplet sensitization. The quantity I_{sat} determines the point at which upconverted fluorescence saturation becomes significant and is highly dependent on the product $k_{sens}[A_0]$. We have also considered the behavior of the local slope *n*, which quantifies the dependence of upconverted fluorescence intensity on the irradiance *I*. It is beneficial for a TTA-UC system to remain in the linear regime, where $n \sim 1$, while avoiding fluorescence signal saturation. Therefore, there exists a region of irradiance through which a TTA-UC system performs most optimally, which we have defined via the quantities Γ and $\log(I_{sat}/I_{th})$. Indeed, we show that an early onset of saturation, which occurs when $I_{sat} \ll I_{th}$, might lead to the false conclusion that the TTA-UC system in question possesses a small I_{th}. Another important consequence of incorporating mass conservation in an analytical TTA model is that the TTA quantum yield is limited by the quantities k_{TTA} and k_T^A, in contrast to what had been thought based on prior kinetic models.

We have also illustrated the difficulty in obtaining I_{th} through a graphical inspection of a logarithmic plot of upconverted fluorescence vs. irradiance. We demonstrated that with a limited dynamic range, it is nearly impossible to observe a complete transition in local slope from a value of 2 to a value of 1. An alternative strategy to determine I_{th}, as well as other useful system parameters, is to fit experimental upconverted fluorescence data with our quadratic model. Our model successfully fits experimental upconverted fluorescence data from a wide range of different systems, although we find that the model is inadequate in replicating the behavior of upconverted fluorescence from TTA-UC gels and devices. Given the inability of I_{th} to make an accurate prediction of the performance of a TTA-UC system that exhibits an early onset of saturation, we have proposed the use of additional figures of merit, and demonstrated their determination from literature data using our fitting method.

It should also be noted that although we have demonstrated our ability to determine I_{th} with our fitting method, we have found that different combinations of system parameters might lead to an equally good fit and near identical values of I_{th}. When armed with a rough knowledge of the critical system parameters k_T^A and k_{sens}, however, fits with unique parameter values can be made. It would be useful in the future to extend the model to include effects such as triplet energy back-transfer from the annihilator to the sensitizer, singlet fission, and an inhomogeneous distribution of sensitizers and annihilators across a sample.

Author contributions

A.K. and J.T.F. developed the kinetic model. A.K. performed all of the calculations and fitting. T.D. performed the experiments. A.K. wrote the manuscript. J.T.F. and K.H. supervised the work and edited the manuscript.

Acknowledgments

This work was supported by the National Science Foundation, grant CHE-1800491 (J.T.F. and A.K.) and DMR-1752782 (K.H. and T.D.). A.K. would also like to thank the University of Maryland's Graduate School and the Department of Materials Science and Engineering for supporting this research through a Summer Graduate Research Fellowship.

References

1. P. P. Feofilov and V. V. Ovsyankin, *Appl. Opt.*, 1967, **6**, 1828-1833.
2. T. N. Singh-Rachford and F. N. Castellano, *Coord. Chem. Rev.*, 2010, **254**, 2560-2573.
3. T. F. Schulze and T. W. Schmidt, *Energ. Environ. Sci.*, 2015, **8**, 103-125.
4. C. A. Parker and C. G. Hatchard, *Proc. R. Soc. A*, 1962, **269**, 574-584.

5. F. Laquai, G. Wegner, C. Im, A. Büsing and S. Heun, *J. Chem. Phys.*, 2005, **123**, 074902.

6. I. Tanaka and S. Tokito, *J. Appl. Phys.*, 2005, **97**, 113532.

7. S. Baluschev, P. E. Keivanidis, G. Wegner, J. Jacob, A. C. Grimsdale, K. Müllen, T. Miteva, A. Yasuda and G. Nelles, *Appl. Phys. Lett.*, 2005, **86**, 061904.

8. M. A. Baldo, M. E. Thompson and S. R. Forrest, *Nature*, 2000, **403**, 750-753.

9. A. Monguzzi, J. Mezyk, F. Scotognella, R. Tubino and F. Meinardi, *Phys. Rev. B*, 2008, **78**, 195112.

10. A. Monguzzi, R. Tubino, S. Hoseinkhani, M. Campione and F. Meinardi, *Phys. Chem. Chem. Phys.*, 2012, **14**, 4322-4332.

11. T. Ogawa, N. Yanai, A. Monguzzi and N. Kimizuka, *Sci. Rep.*, 2015, **5**, 10882.

12. A. Haefele, J. Blumhoff, R. S. Khnayzer and F. N. Castellano, *J. Phys. Chem. Lett.*, 2012, **3**, 299-303.

13. J. E. Auckett, Y. Y. Chen, T. Khoury, R. G. C. R. Clady, N. J. Ekins-Daukes, M. J. Crossley and T. W. Schmidt, *J. Phys. Conf. Ser.*, 2009, **185**, 012002.

14. Y. Y. Cheng, A. Nattestad, T. F. Schulze, R. W. MacQueen, B. Fückel, K. Lips, G. G. Wallace, T. Khoury, M. J. Crossley and T. W. Schmidt, *Chem. Sci.*, 2016, **7**, 559-568.

15. Y. Murakami and K. Kamada, *Phys. Chem. Chem. Phys.*, 2021, **23**, 18268-18282.

16. Y. Y. Cheng, B. Fückel, T. Khoury, R. G. C. R. Clady, M. J. Y. Tayebjee, N. J. Ekins-Daukes, M. J. Crossley and T. W. Schmidt, *J. Phys. Chem. Lett.*, 2010, **1**, 1795-1799.

17. P. Bharmoria, H. Bildirir and K. Moth-Poulsen, *Chem. Soc. Rev.*, 2020, **49**, 6529-6554.

18. D. G. Bossanyi, Y. Sasaki, S. Wang, D. Chekulaev, N. Kimizuka, N. Yanai and J. Clark, *JACS Au*, 2021, **1**, 2188-2201.

19. V. Jankus, M. Aydemir, F. B. Dias and A. P. Monkman, *Adv. Sci.*, 2016, **3**, 1500221.

20. X. Wang, R. Tom, X. Liu, D. N. Congreve and N. Marom, *J. Mater. Chem. C*, 2020, **8**, 10816-10824.

21. H. Lim, S.-J. Woo, Y. H. Ha, Y.-H. Kim and J.-J. Kim, *Adv. Mater.*, 2022, **34**, 2100161.

22. C. Gao, B. Zhang, C. R. Hall, L. Li, Y. Chen, Y. Zeng, T. A. Smith and W. W. H. Wong, *Phys. Chem. Chem. Phys.*, 2020, **22**, 6300-6307.

23. M. Kasha, *Discuss. Faraday Soc.*, 1950, **9**, 14-19.

24. N. Liaros, S. A. Gutierrez Razo, M. D. Thum, H. M. Ogden, A. N. Zeppuhar, S. Wolf, T. Baldacchini, M. J. Kelley, J. S. Petersen, D. E. Falvey, A. S. Mullin and J. T. Fourkas, *iScience*, 2022, **25**, 103600.

25. Y. Zhou, F. N. Castellano, T. W. Schmidt and K. Hanson, *ACS Energy Lett.*, 2020, **5**, 2322-2326.

26. F. Edhborg, A. Olesund and B. Albinsson, *Photochem. Photobiol. Sci.*, 2022, DOI: 10.1007/s43630-022-00219-x.

27. F. Deng, A. J. Francis, W. W. Weare and F. N. Castellano, *Photochem. Photobiol. Sci.*, 2015, **14**, 1265-1270.

28. A. Olesund, V. Gray, J. Mårtensson and B. Albinsson, *J. Amer. Chem. Soc.*, 2021, **143**, 5745-5754.

29. V. Gray, D. Dzebo, A. Lundin, J. Alborzpour, M. Abrahamsson, B. Albinsson and K. Moth-Poulsen, *J. Mater. Chem. C*, 2015, **3**, 11111-11121.

30. D. Lin, J. Zhong, S. Ji, Z. Yuan, L. Xing, Q. He, H. Zhang and Y. Huo, *Dyes Pigm.*, 2021, **185**, 108912.

31. M. Han, Z. Zhu, M. Ouyang, Y. Liu and X. Shu, *Adv. Funct. Mater.*, 2021, **31**, 2104044.

32. V. Gray, A. Dreos, P. Erhart, B. Albinsson, K. Moth-Poulsen and M. Abrahamsson, *Phys. Chem. Chem. Phys.*, 2017, **19**, 10931-10939.

33. Y. Kawashima, H. Kouno, K. Orihashi, K. Nishimura, N. Yanai and N. Kimizuka, *Mol. Syst. Des. Eng.*, 2020, **5**, 792-796.

34. A. L. Hagstrom, H.-L. Lee, M.-S. Lee, H.-S. Choe, J. Jung, B.-G. Park, W.-S. Han, J.-S. Ko, J.-H. Kim and J.-H. Kim, *ACS Appl. Mater. Interfaces*, 2018, **10**, 8985-8992.

35. T.-A. Lin, C. F. Perkinson and M. A. Baldo, *Adv. Mater.*, 2020, **32**, 1908175.

36. Y. Zhou, S. Ayad, C. Ruchlin, V. Posey, S. P. Hill, Q. Wu and K. Hanson, *Phys. Chem. Chem. Phys.*, 2018, **20**, 20513-20524.

37. L. Nienhaus, J.-P. Correa-Baena, S. Wieghold, M. Einzinger, T.-A. Lin, K. E. Shulenberger, N. D. Klein, M. Wu, V. Bulović, T. Buonassisi, M. A. Baldo and M. G. Bawendi, *ACS Energy Lett.*, 2019, **4**, 888-895.

38. A. Ronchi, P. Brazzo, M. Sassi, L. Beverina, J. Pedrini, F. Meinardi and A. Monguzzi, *Phys. Chem. Chem. Phys.*, 2019, **21**, 12353-12359.

39. S. Amemori, Y. Sasaki, N. Yanai and N. Kimizuka, *J. Amer. Chem. Soc.*, 2016, **138**, 8702-8705.

40. M. Wu, D. N. Congreve, M. W. B. Wilson, J. Jean, N. Geva, M. Welborn, T. Van Voorhis, V. Bulović, M. G. Bawendi and M. A. Baldo, *Nat. Photonics*, 2016, **10**, 31-34.

41. R. Vadrucci, A. Monguzzi, F. Saenz, B. D. Wilts, Y. C. Simon and C. Weder, *Adv. Mater.*, 2017, **29**, 1702992.

42. D. F. Barbosa de Mattos, A. Dreos, M. D. Johnstone, A. Runemark, C. Sauvée, V. Gray, K. Moth-Poulsen, H. Sundén and M. Abrahamsson, *J. Chem. Phys.*, 2020, **153**, 214705.

43. S. P. Hill and K. Hanson, *J. Amer. Chem. Soc.*, 2017, **139**, 10988-10991.

44. S. P. Hill, T. Dilbeck, E. Baduell and K. Hanson, *ACS Energy Lett.*, 2016, **1**, 3-8.

45. T. Dilbeck, S. P. Hill and K. Hanson, *J. Mater. Chem. A*, 2017, **5**, 11652-11660.